

Technical note: Characterizing individual milk fat globules with holographic video microscopy

Fook Chiong Cheong, Ke Xiao and David G. Grier*
Department of Physics and Center for Soft Matter Research
New York University, New York, NY 10003

J. Dairy Sci. **92**, 95-99 (2009)

Abstract

We use in-line holography to create images of individual milk fat globules in diluted samples of milk. Analyzing these images with the exact Lorenz-Mie light scattering theory then yields the droplets' radii with nanometer resolution and their refractive indexes to within one part in a thousand. This procedure rapidly and directly characterizes both the quantity and quality of fat in milk.

*Corresponding author: david.grier@nyu.edu

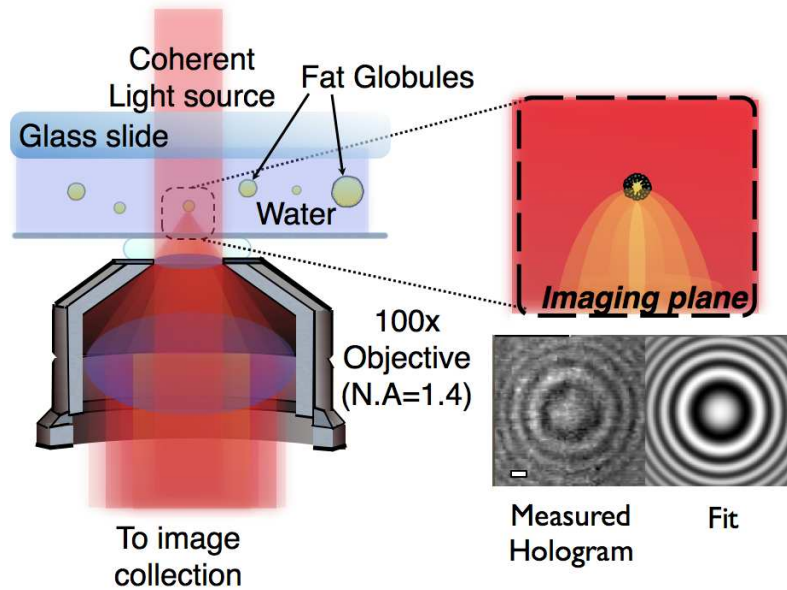


Figure 1: Schematic representation of holographic video microscopy. The sample scatters light from a collimated laser beam. Both the scattered and unscattered laser light are collected by an oil-immersion objective lens and relayed to a video camera, which records their interference as a hologram. A typical example of one fat droplet’s hologram is shown to the right, together with a fit to Eqs. (1) through (6).

Optical characterization methods are widely used to monitor and optimize the properties of milk during processing and packaging (Jääskeläinen et al., 2001). Although rapid and non-invasive, such methods generally provide only an indirect view of such properties as the concentration, size distribution and composition of the milk fat globules in a sample. Holographic video microscopy (Sheng et al., 2006; Lee and Grier, 2007; Lee et al., 2007) offers a complementary and highly quantitative view of individual globules’ optical properties, yet is rapid enough to provide a statistical overview of a bulk sample’s properties. In particular, this method yields the radius of individual globules with nanometer resolution and the refractive index to within one part in a thousand. A statistical sampling of the globule radii provides a direct measurement of a sample’s fat concentration and size distribution. The distribution of refractive indexes is useful for characterizing the globules’ composition, and thus the nature and quality of the milk.

Our holographic microscope, depicted schematically in Fig. 1, is based on a commercial inverted light microscope (Zeiss Axiovert TV 100 S). The conventional incandescent illuminator is replaced with the 3 mm diameter collimated beam from a 10 mW HeNe laser (Uniphase) operating at a vacuum wavelength of $\lambda = 632.8$ nm. Such weak laser irradiation will not appreciably raise the temperature of an aqueous sample.

An individual milk fat globule of radius a at position \mathbf{r}_p scatters a small portion of the plane-wave illumination. The scattered light then propagates to the focal plane of the microscope, where it interferes with the unscattered portion of the laser beam. The resulting interference pattern is magnified by the microscope’s objective lens (S Plan Apo, 100 \times , NA 1.4, oil immersion) and projected by a video eyepiece (0.63 \times) onto a CCD camera (NEC TI-324AII) before being recorded as uncompressed digital video with a digital video recorder (Panasonic DVR-H110).

Each holographic image in the video stream is a time-resolved snapshot of the three-dimensional distribution of scatterers in the microscope’s field of view. We then use results of the Lorenz-Mie theory of light scattering by small particles (Bohren and Huffman, 1983; Barber and Hill, 1990; Mishchenko et al., 2001) to measure each particle’s radius and index of refraction (Lee et al., 2007).

We used this method to analyze milk fat droplets from a range of commercial milk products including several grades of homogenized pasteurized cows’ milk and goats’ milk. In each case, the sample was diluted by 1000:1 with deionized water before being sealed in the 50 μm gap between a microscope slide and a glass cover slip and mounted on the stage of the microscope. Given the imaging system’s calibrated magnification of 101 nm/pixel, a typical 640×480 pixel image, $I(\mathbf{r})$, captures roughly 10 resolvable globules.

Unprocessed holograms suffer from large intensity variations due to speckle, interference effects in the microscope’s optics and scattering by dust and other imperfections. We correct for these by normalizing $I(\mathbf{r})$ with a background hologram $I_0(\mathbf{r})$ obtained with no sample in the field of view. The normalized hologram then can be fit to the prediction of Lorenz-Mie

theory (Bohren and Huffman, 1983; Barber and Hill, 1990; Mishchenko et al., 2001),

$$\frac{I(\mathbf{r})}{I_0(\mathbf{r})} = 1 + 2\alpha \Re \{ \mathbf{f}_s(\mathbf{r} - \mathbf{r}_p) \cdot \hat{\mathbf{e}} e^{-ikz_p} \} + \alpha^2 |\mathbf{f}_s(\mathbf{r} - \mathbf{r}_p)|^2, \quad (1)$$

where $k = 2\pi n_m/\lambda$ is the wavenumber of light in a medium of refractive index n_m , and where $\mathbf{f}_s(\mathbf{r} - \mathbf{r}_p)$ is the Lorenz-Mie scattering function describing how light of polarization $\hat{\mathbf{e}}$ is scattered by a sphere located at \mathbf{r}_p . In practice, the illuminating beam is not perfectly uniform, and the factor $\alpha \approx 1$ can be used to account for position-dependent variations. Assuming the scatterer to be a uniform and homogeneous dielectric sphere illuminated by light that is linearly polarized in the $\hat{\mathbf{x}}$ direction,

$$\mathbf{f}_s(\mathbf{r}) = \sum_{n=1}^{\infty} f_n \left(ia_n \mathbf{N}_{e1n}^{(3)}(\mathbf{r}) - b_n \mathbf{M}_{o1n}^{(3)}(\mathbf{r}) \right), \quad (2)$$

where $f_n = i^n(2n+1)/[n(n+1)]$, and where $\mathbf{M}_{o1n}^{(3)}(\mathbf{r})$ and $\mathbf{N}_{e1n}^{(3)}(\mathbf{r})$ are vector spherical harmonics (Bohren and Huffman, 1983; Barber and Hill, 1990),

$$\mathbf{M}_{o1n}^{(3)}(\mathbf{r}) = \frac{\cos \phi}{\sin \theta} P_n^1(\cos \theta) j_n(kr) \hat{\boldsymbol{\theta}} - \sin \phi \frac{dP_n^1(\cos \theta)}{d\theta} j_n(kr) \hat{\boldsymbol{\phi}} \quad (3)$$

and

$$\begin{aligned} \mathbf{N}_{e1n}^{(3)}(\mathbf{r}) = n(n+1) \cos \phi P_n^1(\cos \theta) \frac{j_n(kr)}{kr} \hat{\mathbf{r}} + \cos \phi \frac{dP_n^1(\cos \theta)}{d\theta} \frac{1}{kr} \frac{d}{dr} [r j_n(kr)] \hat{\boldsymbol{\theta}} \\ - \frac{\sin \phi}{\sin \theta} P_n^1(\cos \theta) \frac{1}{kr} \frac{d}{dr} [r j_n(kr)] \hat{\boldsymbol{\phi}}. \end{aligned} \quad (4)$$

Here, $P_n^1(\cos \theta)$ is the associated Legendre polynomial of the first kind, and $j_n(kr)$ is the spherical Bessel function of the first kind of order n . The expansion coefficients are given by (Bohren and Huffman, 1983)

$$a_n = \frac{m^2 j_n(mka) [ka j_n(ka)]' - j_n(ka) [mka j_n(mka)]'}{m^2 j_n(mka) [ka h_n^{(1)}(ka)]' - h_n^{(1)}(ka) [mka j_n(mka)]'} \quad (5)$$

and

$$b_n = \frac{j_n(mka) [ka j_n(ka)]' - j_n(ka) [mka j_n(mka)]'}{j_n(mka) [ka h_n^{(1)}(ka)]' - h_n^{(1)}(ka) [mka j_n(mka)]'}, \quad (6)$$

where $m = n_p/n_m$ is the particle's refractive index relative to the medium, $j_n(x)$ is the spherical Bessel function of the first type of order n , $h_n^{(1)}(x)$ is the spherical Hankel function of the first type of order n , and where primes denote derivatives with respect to the argument. The sum in Eq. (2) converges after a number of terms, $n_c = ka + 4.05(ka)^{1/3} + 2$, which depends on the particle's size (Barber and Hill, 1990; Mishchenko et al., 2001). The only challenge in this computation is to calculate the Bessel functions and their ratios both accurately and efficiently. We use the accurate, but computationally intensive continued fraction algorithm due to Lentz to compute the a_n and b_n coefficients (Lentz, 1976), and the more efficient recursive algorithm due to Wiscombe for the spherical Bessel functions (Wiscombe, 1980). This trade-off ensures that we can obtain accurate results using our apparatus for spheres ranging in diameter from 10 nm to more than 10 μ m and refractive indexes exceeding $n_p = 2.6$.

To characterize a sphere, we fit its normalized hologram to Eqs. (1) through (6) for the sphere's radius a , its refractive index n_p , its three-dimensional position \mathbf{r}_p , and also α , using a standard Levenberg-Marquardt least-squares algorithm (Moré et al., 1980; Moré, 1977; Gill and Murray, 1978). Despite the fairly large number of free parameters, these fits converge rapidly and robustly, and typically yield the particle's size and position with nanometer-scale resolution, and its refractive index to within one part in a thousand (Lee et al., 2007). Such extreme sub-pixel spatial resolution is possible because information from many pixels contributes to each fit.

We applied this technique to 5 samples of commercially processed milk obtained from a local supermarket. These include pasteurized homogenized cows' milk from Elmherst Dairy (Jamaica, NY) with designated fat contents ranging from fat-free to whole milk, as well as pasteurized homogenized goats' milk from Meyenberg Goat Milk (Turlock, CA). Samples

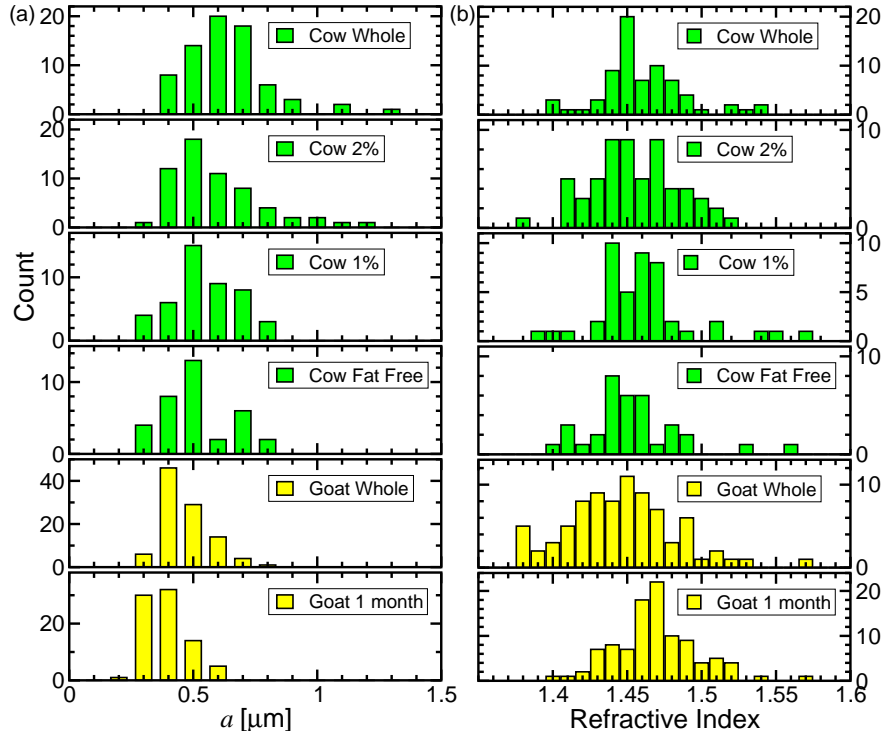


Figure 2: Histograms of fat droplet radii (a) and refractive indexes (b) obtained from single-droplet characterization measurements.

were allowed to equilibrate on the microscope stage to ambient temperature, $T = 23 \pm 1^\circ\text{C}$. Up to 100 randomly selected fat droplets were analyzed for each sample to obtain estimates for the size and refractive index distributions for the fat droplets in each sample. The results are summarized in Fig. 2, Fig. 3 and Table 1. Figure 2 presents histograms of the milk fat globule radii and refractive indexes for each of the samples. The mean values presented in Table 1 are computed as averages of the single-droplet values. Reported errors are the quadrature sum of the standard deviation of the values and the measurement error estimated from the fits.

As might be expected, the average radius of the fat globules in cows' milk is smaller in samples with lower fat content. This is consistent with the creaming process by which fat is removed from whole milk. The mean refractive index of the cows' milk fat globules varies far less from sample to sample. The mean refractive index of $n = 1.464$, averaged over all of the droplets from all of the cows' milk samples, agrees with bulk values obtained by Abbé

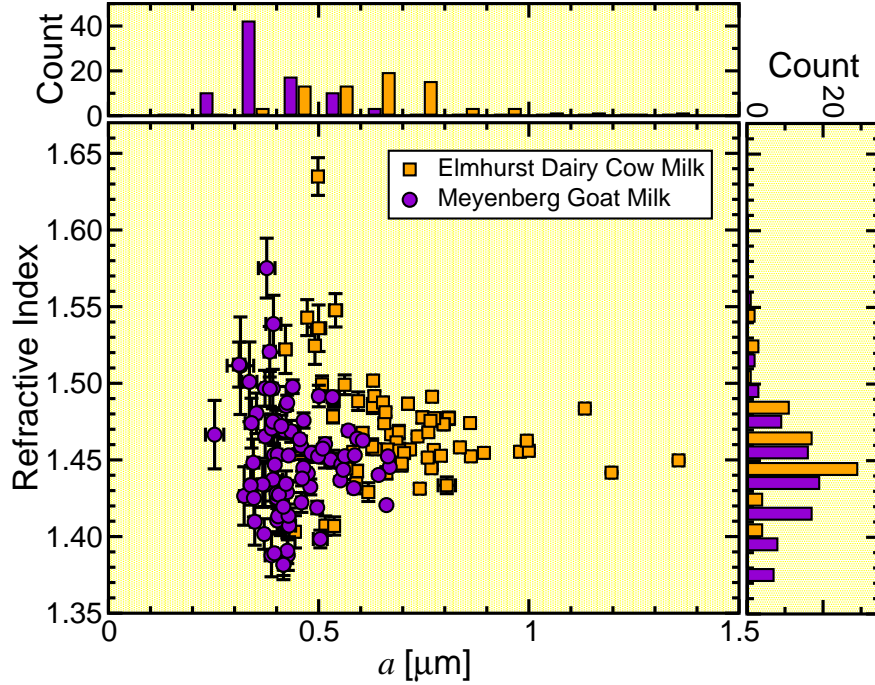


Figure 3: Scatter plot of refractive index and globule radius a for commercial milk samples. Each data point represents results for a single fat droplet. Error bars are computed from the normalized covariance matrix of the fitting parameters. Histograms at the top and side show the number-weighted distribution of values of the radius and refractive index, respectively.

Sample	Radius [μm]	Refractive Index
Cow Whole	0.693 ± 0.174	1.468 ± 0.035
Cow 2%	0.643 ± 0.183	1.460 ± 0.029
Cow 1%	0.590 ± 0.131	1.465 ± 0.034
Cow Fat Free	0.562 ± 0.140	1.460 ± 0.031
Goat Whole	0.576 ± 0.137	1.425 ± 0.038
Goat 1 month	0.441 ± 0.088	1.451 ± 0.036
Type B Immersion Oil		1.521 ± 0.017

Table 1: Globule radius and refractive index for commercial milk samples.

refractometry on melted fat samples (Krukovsky, 1961) and with sample-averaged single-droplet refractive indexes obtained by light scattering (Michalski et al., 2001). This value substantially exceeds the range of 1.3444 to 1.3525 obtained for the overall refractive index of bulk samples (Jääskeläinen et al., 2001), which is dominated by the optical properties of water, whose refractive index at room temperature is $n_m = 1.333$.

Estimating the milk fat globules' refractive index from its contribution to light scattering or conventional refractometry measurements requires accurate information regarding the droplets' concentration and size distribution. Holographic characterization, by contrast, unambiguously quantifies individual droplets' optical properties without recourse to models or ancillary measurements. Because a droplet's refractive index depends on its composition, moreover, these measurements also can be used to characterize the composition and quality of milk samples. Indeed, the data in Table 1 and Fig. 3 demonstrate that it is possible to distinguish goats' milk from cows' milk on this basis, the goats' milk having a resolvably smaller mean refractive index, the difference being confirmed at the 95 percent confidence level by a Welch's t-test.

The high resolution afforded by holographic characterization allows us to track subtle changes in a sample as the milk ages. Table 1 shows that the mean refractive index of goat milk droplets increases over the course of a month, rising from 1.43 to 1.45. This coincides with a decrease in the mean droplet radius from 0.58 μm to 0.44 μm . Both changes are resolved at the 95 confidence level according to Welch's t-test. This result demonstrates that holographic characterization can be useful not only for distinguishing types of milk, but also may be used to assess the age of a sample.

Having access to particle-resolved data also reveals an interesting correlation between the size of the fat globules and the range of their estimated refractive indexes. Larger particles' apparent refractive indexes are consistent with each other to within the resolution of the measurement technique (Lee et al., 2007). Smaller droplets, by contrast, display substantially larger variations in refractive index from droplet to droplet.

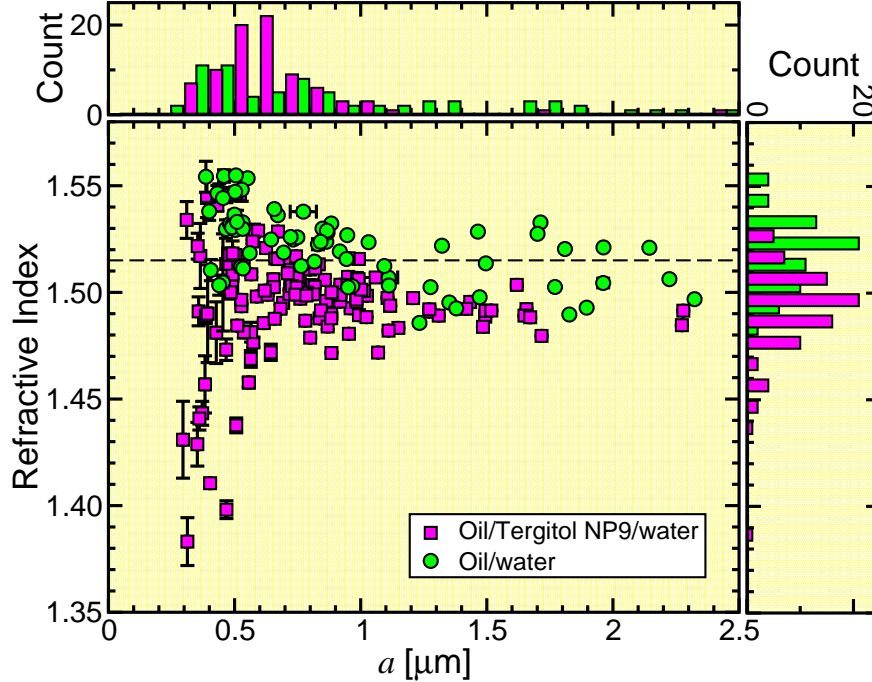


Figure 4: Refractive index versus droplet radius, a , for dispersed Type B immersion oil in water, both with (squares) and without (circles) surfactant.

This is not an inherent limitation of the measurement technique, as the data in Fig. 4 demonstrate. The circular data points in Fig. 4 were obtained for spherical droplets of Cargille Type B microscope immersion oil that were transiently dispersed in deionized water by vigorous shearing and then diluted with deionized water to obtain droplet concentrations and size distributions qualitatively similar to those of the milk samples. Although these surfactant-free dispersions are thermodynamically unstable, their recombination kinetics are sufficiently slow that we are able to obtain clear holograms of the individual droplets before they coalesce. The immersion oil has a nominal bulk refractive index of 1.515 for red light at a temperature of 25°C. The measured values differ from this by no more than 2 percent over the entire range of droplet radii that were sampled.

Results more reminiscent of those for milk fat droplets are obtained when the oil droplets are stabilized with surfactant. The square points in Fig. 4 were obtained for Type B oil with the addition of 0.1% (v/v) Tergitol NP9, a nonionic surfactant whose bulk refractive index is 1.491. The addition of this lower-index surfactant systematically reduces the single-droplet

refractive index for larger particles. It also increases the variability of measured refractive indexes to more than 10 percent for particles with radii smaller than $0.6 \mu\text{m}$.

Because the excess of surfactant guarantees complete coverage of the oil droplets' surfaces, these observations demonstrate that holographic particle characterization is sensitive to surface coverage by surfactants. In the case of milk droplets, this suggests that holographic microscopy is influenced by the optical properties of the milk fat globule membrane (MFGM) (Dewettinck et al., 2007). This sensitivity is noteworthy because, at just 10 to 20 nm thickness, the MFGM is much thinner than the wavelength of light and constitutes a very small proportion of the droplets' volume.

The Lorenz-Mie light scattering formulas in Eq. (2) through (6) are appropriate for a homogeneous isotropic sphere with an abrupt interface. Using this result to interpret holograms of coated spheres consequently can lead to inconsistencies in the extracted parameters. This effect should be more pronounced for smaller spheres whose surface-area-to-volume ratio is higher. Applying a more sophisticated form of the scattering function that accounts for core-shell structure (Bohren and Huffman, 1983; Barber and Hill, 1990) should reduce this variability at the expense of additional computational complexity. The benefit would be the ability to characterize the MFGM.

The basic implementation of holographic droplet characterization presented here provides a droplet-by-droplet analysis of milk fat droplets' sizes and also their refractive indexes at a particular wavelength of light. This information, in turn, offers insights into the droplets' composition, for example enabling us to distinguish goats' milk from cows' milk. Holographic characterization can be extended to multiple wavelengths, which would provide true spectroscopic information on milk fat globules' composition. This technique requires little specialized equipment, and so can be easily adapted for process control and quality assurance applications.

We are grateful to Osman Akcikir for bringing Lentz (1976) to our attention. This work was supported by the National Science Foundation under Grant Number DMR-0606415.

References

- Barber, P. W. and S. C. Hill, 1990. Light Scattering by Particles: Computational Methods, volume 2 of *Advanced Series in Applied Physics*. World Scientific, New Jersey.
- Bohren, C. F. and D. R. Huffman, 1983. Absorption and Scattering of Light by Small Particles. Wiley Interscience, New York.
- Dewettinck, K., R. Rombaut, N. Thienpont, T. T. Le, K. Messens, and J. Van Camp, 2007. Nutritional and technological aspects of milk fat globule membrane. *Int. Dairy J.* 18:436–457.
- Gill, P. E. and W. Murray, 1978. Algorithms for the solution of the nonlinear least-squares problem. *SIAM J. Numer. Anal.* 15:977–992.
- Jääskeläinen, A. J., K.-E. Peiponen, and J. A. Rätty, 2001. On reflectometric measurement of a refractive index of milk. *J. Dairy Sci.* 84:38–43.
- Krukovsky, V. N., 1961. Vitamin A, carotenoid, iodine, and thiocyanogen values, and the refractive index of milk fat as influenced by feed, and by individual and breed differences. *J. Ag. Food Chem.* 9:326–330.
- Lee, S.-H. and D. G. Grier, 2007. Holographic microscopy of holographically trapped three-dimensional structures. *Opt. Express* 15:1505–1512.
- Lee, S.-H., Y. Roichman, G.-R. Yi, S.-H. Kim, S.-M. Yang, A. van Blaaderen, P. van Oostrum, and D. G. Grier, 2007. Characterizing and tracking single colloidal particles with video holographic microscopy. *Opt. Express* 15:18275–18282.
- Lentz, W. J., 1976. Generating Bessel functions in Mie scattering calculations using continued fractions. *Appl. Opt.* 15:668–671.
- Michalski, M.-C., V. Briard, and F. Michel, 2001. Optical parameters of milk fat globules for laser light scattering measurements. *Lait* 81:787–796.

- Mishchenko, M. I., L. D. Travis, and A. A. Lacis, 2001. *Scattering, Absorption and Emission of Light by Small Particles*. Cambridge University Press, Cambridge.
- Moré, J. J., 1977. The Levenberg-Marquardt algorithm: Implementation and theory. In G. A. Watson, editor, *Numerical Analysis, Lecture Notes in Mathematics 630*. Springer-Verlag, Berlin.
- Moré, J. J., B. S. Garbow, and K. E. Hillstom, 1980. User guide for MINPACK-1. Technical Report ANL-80-74, Argonne National Laboratory, Argonne, IL.
- Sheng, J., E. Malkiel, and J. Katz, 2006. Digital holographic microscope for measuring three-dimensional particle distributions and motions. *Appl. Opt.* 45:3893–3901.
- Wiscombe, W. J., 1980. Improved Mie scattering algorithms. *Appl. Opt.* 19:1505–1509.